IEEE Access
Multidisciplinary ⋮ Rapid Review ⋮ Open Access Journal

Received August 29, 2020, accepted September 25, 2020, date of publication September 30, 2020, date of current version October 13, 2020.

Digital Object Identifier 10.1109/ACCESS.2020.3027817

Investigation on the Impact-Based Energy Conversion of a Dielectric Elastomer Membrane

XI-XIN RAO[1,2], CAI-LIANG ZHANG[1,2], LI-KUAN ZHU[1], GUO-QING ZHANG[1], JIAN-WEI ZHANG[2], AND ZHI-HUI LAI[1]

[1]Guangdong Provincial Key Laboratory of Micro/Nano Optomechatronics Engineering, College of Mechatronics and Control Engineering, Shenzhen University, Shenzhen 518060, China
[2]School of Mechatronics Engineering, Nanchang University, Nanchang 330031, China

Corresponding author: Zhi-Hui Lai (laizh@szu.edu.cn)

This work was supported in part by the National Natural Science Foundation of China under Grant 51905349, in part by the Natural Science Foundation of Guangdong Province under Grant 2020A1515011509, and in part by the Natural Science Foundation of Shenzhen University under Grant 2019036 and Grant 860-000002110264.

ABSTRACT Dielectric elastomer generators (DEGs) provide a new solution for vibrational energy harvesting. Currently, a type of impact-based DEGs, which can harvest energy from ambient vibrations, has been proposed and studied through simulations. However, the energy conversion mechanism and the performance evaluation approach of such impact-based DEGs have not been fully studied yet, thus limiting the reliability of the research on the system design/optimization and performance evaluation. In this paper, a single-sided impact (SSI) model is proposed to reveal the impact-based energy conversion mechanism. Based on this model, a complete four-stage impact process is analyzed to reveal the energy conversion mechanism, and the electrical outputs and energy conversion efficiency are derived as the energy harvesting performance evaluation indexes. To use the developed analytical model to predict the system electrical response accurately, some important parameters including the coefficient of restitution (COR) and largest deflection of the membrane at impacts were obtained experimentally, and the system output voltages at impacts were measured to verify the theoretical approaches in calculating the system electrical outputs and studying the parameters' influences. Furthermore, the influences of the pre-stretched ratio, impact velocity, and input voltage on the system energy harvesting performance are studied through simulations. The research results can provide guidelines to improve the energy harvesting performance of the impact-based DEGs in real applications.

INDEX TERMS Single-sided impact model, dielectric elastomer, energy harvesting, electrical outputs, energy conversion efficiency.

I. INTRODUCTION

As is well-known, energy crises are becoming a worldwide problem. Researchers around the world are actively exploring green sustainable energy and developing corresponding energy conversion devices. Environmental green energies include energies from wind, solar, wave, tidal, and vibration sources. Among all of them, vibrations can be easily found in a variety of machinery, human movement, building, and other civil structures [1]. Vibrational energy harvesting (VEH) devices can achieve a relatively high energy density at low cost and with various scales, especially small and micro sizes [2]. This makes these devices suitable for many applications such as wireless sensors [3], wearable devices [4], automotive [5], and other sectors [6], [7].

There are several conventional methods to converte vibrational energy into electricity including electromagnetic (EM), electrostatic (ES), triboelectric (TE), and piezoelectricity (PE). The EM VEH devices, which are based on Faraday's law of induction [8], [9], are not suitable for micro and small-scale applications due to their low power density. Traditional ES VEH devices consist of a fixed plate and a movable

The associate editor coordinating the review of this manuscript and approving it for publication was Yunlong Cai.

one connected to a vibrating body, thus realizing a vibration-induced variable capacitor [10], [11]. This method has also been of limited applicability because it can only produce a rather low energy density due to the limitations of the materials, for example, a low dielectric permittivity of the air. The TE VEH devices, which are based on the triboelectric effect between the contact and separation of two contact surfaces [12], can produce a relatively high energy density with relatively low manufacturing costs. However, their durability and output stability are insufficient for a good energy harvester [13]. Thus, up to now the PE VEH devices, which have a simple structure and a relatively high energy conversion efficiency [14], [15], have been focused [16]–[18]. They have been widely used in many applications such as roadway energy harvesting [19], wind energy harvesting [20]–[22], and vibrational energy harvesting [23]–[26]. However, these devices are less versatile than desired and have certain limitations and shortcomings, one of which is their ability to generate only a relatively small power density [2]. These factors restrict the areas of application of PE VEH devices.

In recent years, dielectric elastomers (DE) materials have attracted increasing interests due to their advantages of high energy density, large deformability, good electromechanical conversion efficiency, and moderate or low cost, etc. [27]. Up to now, DE has also shown its application potentials in actuators [28], [29], humanlike robots [30], stretchable electronics [31], energy harvesters [32], and among others. Compared with PE-based energy harvesters, dielectric elastomer generators (DEGs) can convert linear, nonlinear, or rotational motion within a wide frequency range [33]. The major advantages of DEGs also include their high energy density (up to 400 J/kg) [34] and power density (3.8 μW/mm^3) [35], both of which are much higher than those of the EM, ES, and PE energy harvesters [34], [36]–[38].

A DEG works as a variable capacitance [39], [40]. Up to now, several DE-based VEH devices have been developed such as the ocean wave generator [41], wind energy harvester [42], [43], and heel like strike generator [44], etc. However, most of the proposed DEGs utilize the properties of DE membranes (DEMs), which undergo the in-plane deformation. These DEGs with in-plane deformations have structural limitations, which make them unsuitable for a practical vibrational environment. Therefore, such DEGs have not achieved desirable results. On the other side, several DEGs based on the DEMs' out-of-plane deformations, including contact-type DE energy harvester [45], oscillating water column wave energy converter [46], resonant wave energy harvester [47] and rotational energy harvester [48], have been proposed recently and successfully applied in energy harvesting. However, these DEGs cannot be used directly in vibrational energy harvesting. Currently, a type of impact-based DEGs, such as the vibro-impact (VI) DEG system proposed by the authors previously [49]–[52], appeared in the past years providing a novel design for DE-based VEH. Especially, the authors have proposed a galloping-based wind energy harvester with a VI DEG [42]. In this work a simple impact experiment was conducted to identify the dielectric elastomer membrane's dielectric permittivity, coefficient of restitution and largest deflection against impact speed. These parameters were sufficient to analyze the system's dynamical and electrical behaviors under wind environment. The previously mentioned research results based on the VI DEG have shown that the impact-based DEGs are expected to work in practical vibrational environments and achieve high electrical power. However, it must be noted that in the preliminary research, the impact-based energy conversion process has not been fully revealed, and only the output voltage of the system at each impact was considered, which means that the VEH performance of the impact-based DEGs cannot be evaluated reasonably. Moreover, these studies focused on the numerical simulations where some values of the parameters were roughly estimated, leading to the system output results being not accurate enough. Therefore, it is necessary to further analyze the impact-based energy conversion process theoretically and conduct dynamics/electrical experiments to determine the key parameters and verify the theoretical model, thus revealing the VEH mechanism and proposing reasonable indexes to evaluate the VEH performance of the impact-based DEGs.

In this paper, a single-sided impact model was proposed to fully study the impact-based energy conversion process and performance of a DEM. In Section II, a single-sided impact (SSI) model based on the free fall of a ball is proposed, and the detailed energy conversion process at an impact is analyzed with the electrical outputs and the energy conversion efficiency being derived. Several key parameters including the coefficient of restitution (COR) and largest deflection at impacts are determined through a set of experiments in Section III. In Section IV, the electrical outputs and the energy conversion efficiency of the SSI model are calculated and the influences of the pre-stretched ratio, impact velocity, and input voltage are presented. Conclusions are drawn in Section V.

II. THEORETICAL ANALYSIS

A. ANALYSIS OF THE IMPACT-BASED ENERGY CONVERSION PROCESS OF A DEM

A classical DEG consists of a thin dielectric elastomer membrane (DEM) sandwiched between two electrodes. Electrical energy can be gained through the capacitance changes of the DEM during its deformation-recovery process. Previous studies have shown that the impact-based DEGs, e.g., the VI DEG proposed by the authors earlier, have potential advantages compared with other types of DEGs, such as a greater energy density and a higher output power [53]. However, the impact-based energy conversion process has not been fully revealed and the energy harvesting (EH) performance cannot be evaluated reasonably, and the simulation results for such DEGs are not accurate enough due to the inaccurate parameter values.

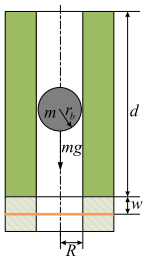

FIGURE 1. The structure of the single-sided impact model based on the free fall of a ball.

To analyze the energy conversion process occurring in the impact-based DEGs, a single-sided impact (SSI) model based on the free fall of a ball is considered in this paper. As shown in Fig. 1, this model comprises a vertical hollow cylinder, an inner rigid ball, and a pre-stretched circular DEM at the bottom of the cylinder. The DEM, which is fixed between two identical cylindrical frames connected to the cylinder, is sandwiched between two compliant electrodes with wires connected to both sides of the DEM. It is easy to imagine that the ball can drop from the top of the cylinder and impact the DEM at the bottom after a free fall. It can be understood that the energy conversion mechanism of this model is the same as that of the impact-based DEGs such as the VI DEG, and the impacts of this model provide a simplification for the impact behaviors of the impact-based DEGs. Thus, using this model, the energy conversion process of the DEM under impacts can be analyzed and the energy conversion performances can be studied quantitatively based on thorough theoretical and experimental investigations. It should be first pointed out that although the ball will impact the DEM several times due to its gravity, we only consider the energy conversion process at the first impact because the following impacts result in similar energy conversion processes.

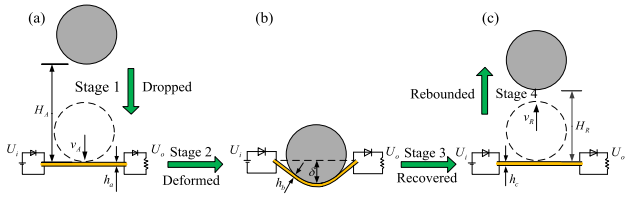

FIGURE 2. The energy conversion process of the SSI model at the first impact, including (a) the dropping process, (b) the largest deformation stage, and (c) the rebounding process.

The (first) impact between the ball and the DEM can be regarded as an inelastic impact with the energy exchange within a short time. A complete impact process involving the free fall consists of four stages, as shown in Fig. 2. At stage 1, the ball of mass m drops from a given height H_A until it contacts the DEM. During this stage, the gravitational potential energy of the sphere is converted into kinetic energy. Stage 2 can be considered as a deformation stage, where the ball's contact force suffered from the DEM gradually increases from 0 to its maximum value, and the ball's velocity reduces to zero when the DEM reaches its largest deformation, which is indicated by the largest deflection δ of the DEM at its center. During this stage, the whole kinetic energy and a bit of gravitational potential energy of the ball are converted into the elastic energy of the DEM with some inevitable energy dissipation during the deformation. Meanwhile, an input voltage is applied on the DEM to provide initial charges when the DEM reaches its largest deformation. Stage 3 represents a recovery stage where the elastic energy stored in the DEM is released. A portion of the elastic energy is converted to the kinetic energy of the ball when it detaches from the upper surface of the DEM; another portion is used to overcome the electric field force across the DEM and higher electrical energy can be achieved; the rest is dissipated during the recovery. At stage 4, the ball runs away from the DEM and reaches a maximum rebound height H_R. During this stage, the kinetic energy of the ball is converted into its gravitational potential energy. In the following theoretical analysis, the charge leakage and the air resistance are assumed to be ignored [54], and the DEM is considered to be fully recovered at the end of each impact. Thus, the energy conversion equations of the four stages during one complete impact process can be obtained according to previous analyses:

$$\begin{cases} mgH_A = \dfrac{1}{2}mv_A^2 & (1.1) \\ \dfrac{1}{2}mv_A^2 + mg\delta = E + T_1 & (1.2) \\ E + W_i = \dfrac{1}{2}mv_R^2 + T_2 + W_0 + mg\delta & (1.3) \\ \dfrac{1}{2}mv_R^2 = mgH_R & (1.4) \end{cases} \tag{1}$$

Here, v_A and v_R are the impact and rebound velocities of the ball; E is the largest elastic energy stored in the DEM; T_1 and T_2 are the energy dissipation during the deformation and recovery stages, respectively; W_i and W_o represent the input/output electrical energies of the SSI model.

In the following of this section, the electrical outputs of the SSI model at the first impact, including the output voltage, electrical energy increment, harvested energy density and harvested specific energy, are obtained through the dimensional and electrical parameter analysis, and the energy conversion efficiency is calculated by analyzing the energy conversion equations. Thus, the energy harvesting mechanism of the impact-based DEGs can be fully revealed.

B. PARAMETRIC ANALYSIS OF THE SSI MODEL

To study the electrical outputs of the SSI model at the first impact, the dimensional parameters of the DEM at different stages shown in Fig. 2 are analyzed first in this subsection. The original area and thickness of the pre-stretched DEM are $A_a = \pi R^2$ and h_a, respectively. At the largest deformation of the DEM shown in Fig. 2(b), the DEM achieves its maximal area A_b and minimal thickness h_b. The area can be obtained by [55]

$$A_b = \frac{\pi(R^2 - (r_b \sin\alpha)^2)}{\cos\alpha} + 2\pi r_b^2(1 - \cos\alpha) \tag{2}$$

where R is the radius of the DEM, and r_b is that of the ball. The value of α at the largest deformation is determined by δ and the system dimensions:

$$\begin{cases} \cos\alpha = \dfrac{r_b(r_b-\delta)+R\sqrt{R^2+\delta^2-2\delta r_b}}{R^2+(r_b-\delta)^2} \\ \sin\alpha = \sqrt{1-\cos^2\alpha} \quad (0 \le \alpha \le 90^\circ) \end{cases} \tag{3}$$

Thus, the value of h_b can be obtained accordingly:

$$h_b = \frac{\pi R^2 h_a}{A_b} \tag{4}$$

The maximal capacitance of the DEM at one impact can be further obtained [42]:

$$C_b = \frac{\varepsilon_0 \varepsilon_r A_b}{h_b} = \frac{\varepsilon_0 \varepsilon_r V}{h_b^2} \tag{5}$$

where $\varepsilon_0 = 8.85 \times 10^{-12}$ is the vacuum permittivity; V is the DEM's constant volume; ε_r is the DEM's relative permittivity, which has been validated in [42] and is given by [56]:

$$\varepsilon_r = \varepsilon(T, \lambda) = a\lambda^2 + b/Te + c \tag{6}$$

where Te is the environment temperature, and λ is the DEM's pre-stretched ratio in terms of its radial direction; $a = -0.053$, $b = 638$ K and $c = 3.024$ are empirical constants.

It can be seen from (4) and (5) that h_b and C_b are governed by A_b, which is a function of δ. It should be noted that δ at each impact is related to the impact velocity and the material stiffness, which is also influenced by the pre-stretched ratio. These relationships will be studied through experiments in the next section of this paper.

When the DEM recovers to its original shape after each impact (see Fig. 2(c)), its capacitance changes back to:

$$C_c = \frac{\varepsilon_0 \varepsilon_r V}{h_c^2} \tag{7}$$

Here, the value of h_c equals to that of h_a.

C. ELECTRICAL OUTPUTS AND ENERGY CONVERSION EFFICIENCY OF THE SSI MODEL

By combining (1.2) and (1.3), the kinetic energy loss at the first impact can be obtained:

$$\Delta K = \frac{1}{2}mv_A^2 - \frac{1}{2}mv_R^2 = T + \Delta W \tag{8}$$

where $T = T_1 + T_2$ represents the total internal energy dissipation at the deformation and recovery stages of the DEM; it should be noted that the value of T depend on the impact velocity and largest deformation of the DEM when other factors such as material type and temperature are given [57]; $\Delta W = W_o - W_i$ indicates the electrical energy increment of the SSI model at the first impact.

Note that the values of v_A and v_R have an intrinsic relationship of $r = -v_R/v_A$, where r indicates the coefficient of restitution (COR) of the DEM at ball's impact [58]:

$$r = \left|\frac{v_R}{v_A}\right| \approx \sqrt{\frac{2gH_R}{2gH_A}} = \sqrt{\frac{H_R}{H_A}} \tag{9}$$

Hence, the kinetic energy loss can be also calculated as:

$$\Delta K = \frac{1}{2}mv_A^2 - \frac{1}{2}mv_R^2 = \frac{1}{2}mv_A^2 \quad (1-r^2) \tag{10}$$

During the recovery stage of the DEM, an input voltage U_i is applied by using an external power supply. A higher output voltage can be obtained after the recovery stage:

$$U_o = \frac{Q}{C_c} = \frac{U_i C_b}{C_c} = \frac{U_i h_c^2}{h_b^2} = \frac{U_i A_b^2}{A_c^2} \tag{11}$$

where $Q = C_b U_i$ indicates the charges stored across the DEM. Moreover, during the recovery stage, the DEM does negative work to overcome the electric field force, thus producing an electrical energy gain across the DEM. The electric field force $F(h)$ can be expressed as:

$$F(h) = QE(h) \tag{12}$$

where h is the thickness of the DEM during the recovery stage, and $E(h)$ the electrical field intensity, which can be calculated as:

$$E(h) = \frac{Q}{\varepsilon_0 \varepsilon_r A} = \frac{C_b U_i}{\varepsilon_0 \varepsilon_r V} h \tag{13}$$

Substituting (5) and (13) into (12), $F(h)$ can be further written as:

$$F(h) = \frac{\varepsilon_r \varepsilon_0 V U_i^2 h}{h_b^4} \tag{14}$$

Thus, the electrical energy increment during the recovery stage can be obtained:

$$\Delta W = \int_{h_b}^{h_c} F(h)dh = \int_{h_b}^{h_c} \frac{\varepsilon_r \varepsilon_0 V U_i^2 h}{h_b^4} dh = \frac{\varepsilon_r \varepsilon_0 V U_i^2 (h_c^2 - h_b^2)}{2h_b^4} \tag{15}$$

Notably, (15) can be also obtained from $\Delta W = C_c U_o^2/2 - C_b U_i^2/2$.

Furthermore, the harvested energy density $ED = \Delta W/V$ (averaged harvested energy over unit volume) and harvested specific energy $SE = \Delta W/M$ (averaged harvested energy over unit mass) of the SSI model at the first impact are defined, where M is the DEM's mass that can be measured by a weighing device. These two parameters combined with the output voltage U_o and the electrical energy increment ΔW are regarded as the electrical outputs of the SSI model at its first impact in this paper.

Finally, the energy conversion efficiency of the SSI model at each impact can be further obtained:

$$\begin{aligned} \eta &= \frac{\Delta W}{\Delta K} = \frac{C_c U_o^2 - C_c U_o U_i}{mv_A^2(1-r^2)} \times 100\% \\ &= \frac{\varepsilon_r \varepsilon_0 V U_i^2 (h_c^2 - h_b^2)}{mh_b^4 v_A^2 (1-r^2)} \times 100\% \end{aligned} \tag{16}$$

Here, two equivalent formulas are provided to calculate the energy conversion efficiency. The first formula can be used to calculate the energy conversion based on the experimental data, while the second one is helpful to predict the energy conversion efficiency theoretically.

It can be seen from the theoretical analysis that r and δ are two key intermediate variables in calculating the impact-based energy conversion performance. In this paper, the calculating approaches for the values of r and δ will be obtained through experiments in the next section.

III. EXPERIMENTAL STUDIES

It has been stated in Section II that, to calculate the electrical outputs and the energy conversion efficiency of the SSI model at each impact, it is necessary to identify the values of r and δ through a set of experiments. Moreover, the output voltage at one impact, which is the main output parameter to calculate other electrical outputs and the energy conversion efficiency, should be measured through experiments and compared with theoretical results, thus verifying the reliability of the analytical model. The conducted experiments and obtained results are presented detailed in this section.

In this work, all the DEM specimens used in experiments were fabricated using VHB 4910 membranes (3M Corporation) with initial radius $R_0 = 10$ mm and thickness $h_0 = 1$ mm. The membranes were radially pre-stretched, attached with copper sheets, clamped using two identical home-made circular frames with inner radius of $R = 6$ mm, and coated with graphene electrodes (Tan Feng Technology) [45]. The basic parameters of the DEM specimens are summarized in Table 1.

TABLE 1. Basic parameters of the specimen used in experiments.

Sample No.	1	2	3	4	5
λ	2	2.5	3	3.5	4
h_a (mm)	0.25	0.16	0.11	0.08	0.06
R (mm)	6	6	6	6	6

A. IMPACT EXPERIMENT

An impact experimental set-up, which is shown in Fig. 3, has been proposed by the authors previously to study the relationships of the membrane's COR (r) and its largest deflection (δ) as functions of impact velocity [42]. In this work, the proposed impact tests were further carried out to fully study the influences of the pre-stretched ratio (λ), impact velocity (v_A), and input voltage (U_i) on these two parameters (r and δ). It can be seen from Fig. 3 that the experimental set-up consisting of a ball ($m = 3.5$ g) and a fixed pre-stretched DEM can be regarded as an SSI model shown in Fig. 1. At each test, the drop height (H_A) can be controlled precisely by the electromagnet connected to a crossbar, and the rebound height (H_R) of the ball at its first impact can be measured by the camera. Thus, the value of r can be calculated according to (9). Moreover, the deflection

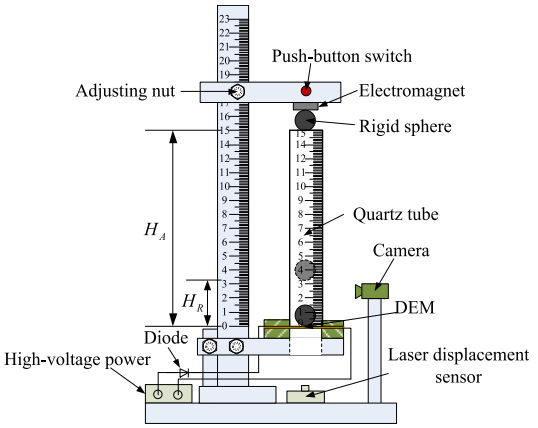

FIGURE 3. The schematic diagram of the impact experiment apparatus to measure the COR and largest deflection of the DEM at impacts.

of the DEM's center can be measured using a laser displacement sensor (Panasonic HG-C1100), thus obtaining the largest deflection at each impact. In this work, experiments were conducted by setting different pre-stretched ratios λ, impact velocities v_A (produced by the different drop heights: $v_A = \sqrt{2gH_A}$), and input voltages U_i. To reduce the measurement errors, five tests were conducted for every parameter set and the measurement results are averaged accordingly.

First, the CORs of the DEM under different λ, v_A and U_i are studied experimentally. The experimental results are shown in Fig. 4. It can be seen from Fig. 4(a) that the COR of the DEM presents an increasing trend as the pre-stretched ratio increases when the impact velocity and input voltage are constants. This can be explained that a larger pre-stretched ratio results in smaller thicknesses during the deformation and recovery process, thus decreasing the energy dissipation [59]. Therefore, a higher rebound height H_R can be achieved and the COR is enhanced according to (9). Fig. 4(b) demonstrates that the COR decreases as the impact velocity increases with the rest parameters kept constant. This can be easily understood that under a larger impact velocity, which results from a higher H_A, the DEM (which is a type of visco-elastic material) will be deformed more and more energy will be dissipated during the deformation and recovery process, thus resulting in a lower rebound height H_R and decreasing the COR according to (9). It is shown in Fig. 4(c) that the COR also presents a decreasing trend as the input voltage increases. The explanation of this trend will be presented later after we illustrate the relation between the input voltage and the largest deflection.

To obtain the quantitative relationships between the COR and these three parameters for further calculations of the electrical outputs and energy conversion efficiency, the experimental data is fitted using the Matlab software and the following equations are obtained under given parameters:

$$r(\lambda) = 0.0618\lambda + 0.1427 \quad (v_A = 1.4 \text{ m/s}, U_i = 2000 \text{ V}) \tag{17}$$

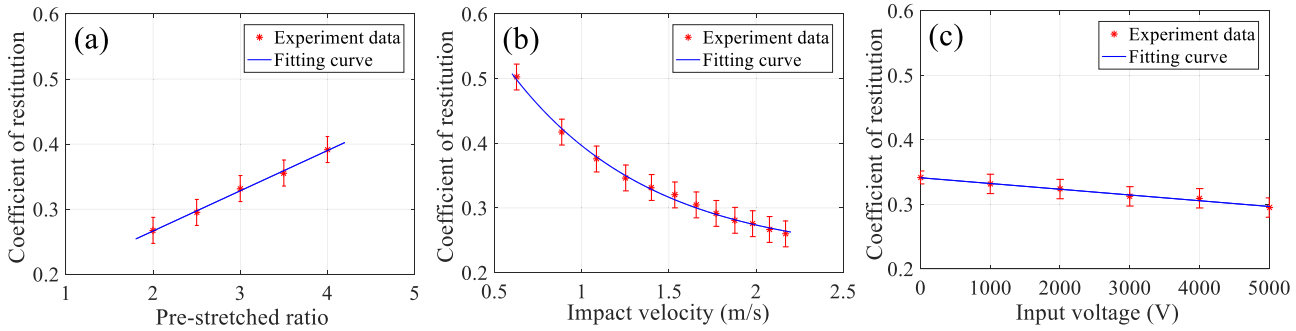

FIGURE 4. COR of the DEM against (a) pre-stretched ratio (H_A = 100 mm (v_A = 1.4 m/s), U_i = 2000 V), (b) impact velocity (λ = 3, U_i = 2000 V) and (c) input voltage(λ = 3, H_A = 100 mm (v_A = 1.4 m/s)).

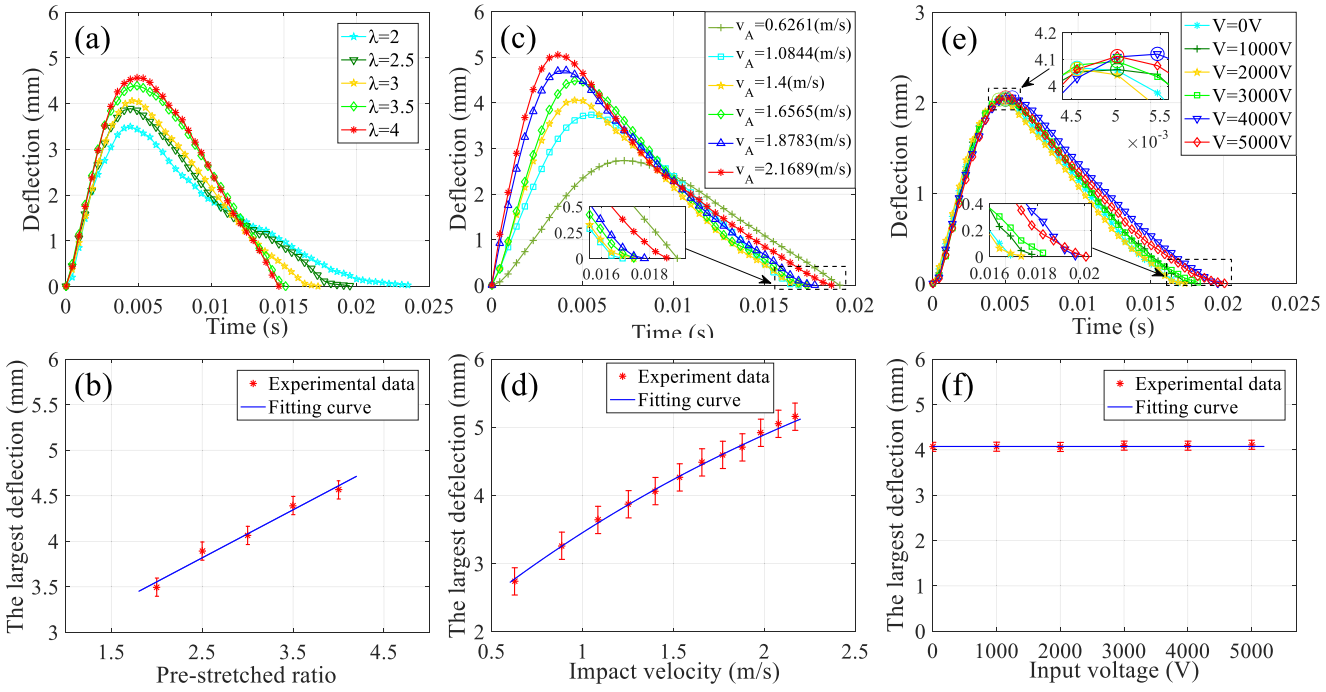

FIGURE 5. (a) Deflection-time curves and (b) the largest deflections under different pre-stretched ratios (H_A = 100 mm (v_A = 1.4 m/s), U_i = 2000 V); (c) deflection-time curves and (d) the largest deflections under different impact velocities (λ = 3, U_i = 2000 V); (e) deflection-time curves and (f) the largest deflections under different input voltages (λ = 3, H_A = 100 mm (v_A = 1.4 m/s)).

$$r(v_A) = 0.5989e^{-1.31v_A} + 0.2241 \quad (\lambda = 3, U_i = 2000\ \text{V}) \tag{18}$$

$$r(U_i) = -8.8979 \times 10^{-6}U_i + 0.3412 \quad (\lambda = 3, v_A = 1.4\ \text{m/s}) \tag{19}$$

Next, the largest deflections of the DEM under different λ, v_A and U_i are studied. Fig. 5(a) presents the deflection of the DEM against time, and the largest deflections under different pre-stretching ratios are plotted in Fig. 5(b). It can be seen from Fig. 5(a) that the impact time (the time interval between two zero-crossing points of the curve) decreases as the pre-stretched ratio increases. Fig. 5(b) shows that the largest deflection of the DEM linearly increases as the pre-stretched ratio increases. The relationship can be obtained by fitting the experimental data with $\delta(\lambda) = a\lambda + b$ and the following equation can be obtained under v_A = 1.4 m/s and U_i = 2000 V:

$$\delta(\lambda) = 5.2738 \times 10^{-4}\lambda + 0.0025 \tag{20}$$

Similar figures are presented in Fig. 5(c, d) for different impact velocities and Fig. 5(e, f) for different input voltages. In Fig. 5(c), it should be noted that to better present the difference between the impact times and largest deflections, only six sets of data were selected from all experimental data. It is can be seen from Fig. 5(c) that the impact time behaves almost like a constant under different impact velocities, and Fig. 5(d) tells that the largest deflection of the DEM exponentially increases as the impact velocity increases. Thus, $\delta(v_A) = ae^{bv_A} + c$ is used to fit the experimental data

and the following equation can be obtained under $\lambda = 3$, $U_i = 2000$ V:

$$\delta(v_A) = -0.0069e^{-0.3498v_A} + 0.0083 \tag{21}$$

One can see from Fig. 5(e, f) that both the impact time and the largest deflection are kept constant under different input voltages. This result indicates that the change of U_i does not affect δ and total internal energy dissipation T when other parameters are kept constant. As U_i increases, we learn from (15) that ΔW will increase. Thus, ΔK will increase according to (8) and r will decrease according to (10), and the increasing of the input voltage results in the decreasing of COR, which accords with the thend of the curve presented in Fig. 4(c).

B. OUTPUT VOLTAGE MEASUREMENT EXPERIMENT

The output voltage of the SSI model at one impact is a key parameter to evaluate the system energy conversion performance and further calculate other electrical outputs. In this subsection, the output voltage measurement experiments were conducted to verify the theoretical approach of (11) in calculating the system output voltage. Moreover, The energy conversion efficiencies are calculated based on the experimental data and are compared with the theoretical results, thus further verifying the proposed analytical model.

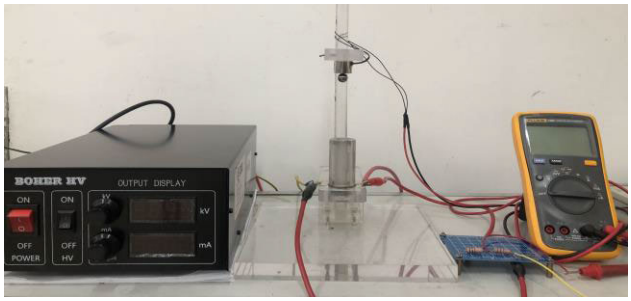

FIGURE 6. The output voltage measurement test system of the SSI model.

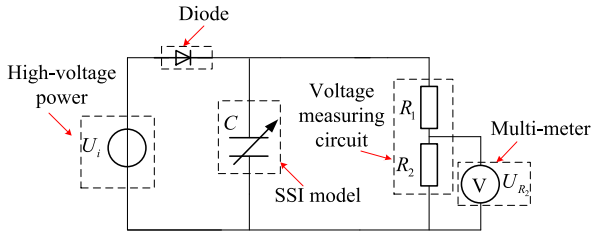

FIGURE 7. The schematic diagram of the output voltage measurement system.

The output voltage measurement system and its schematic diagram are shown in Fig. 6 and Fig. 7, respectively. This system consists of an SSI model, a high-voltage power supply (BOHER 71030P) providing input voltage, a diode preventing the charges flowing back to the power supply, a voltage measuring circuit used to make the output voltage measurable, and a multi-meter used to measure the output voltages of the DEM. In Fig. 7, U_i indicates the constant input voltage; the resistances $R_1 = 1 \times 10^9$ Ω, and $R_2 = 1 \times 10^6$ Ω. Thus, the output voltage of the DEG can be calculated as $U_o \approx 1000U(R_2)$, where $U(R_2)$ is the measured voltages across R_2 when the SSI model generates higher output voltage.

Based on the proposed output voltage measurement system, the output voltages of the SSI model at the ball's first impact under different pre-stretched ratios, impact velocities, and input voltages were measured and recorded, as shown in Fig. 8. It is noted that to avoid the measurement error, each test was carried out ten times, thus obtaining the averaged output voltage with the error-bar indicating the maximum and minimum output voltages. First, Fig. 8(a) shows the test results of output voltages under different pre-stretched ratios. In the tests the input voltage was $U_i = 2000$ V and the drop height was $H_A = 100$ mm ($v_A = 1.4$ m/s). One can see from Fig. 8(a) that higher output voltages are produced, thus verifying the effectiveness of the impact-based energy harvesting of DE materials. It should be pointed out that due to the leakage of the charge, the energy dissipation from the energy harvesting circuit, and not compliant electrodes, etc., the measured output voltages were oscillating and were smaller than the theoretically predicted results [45]. However, it can be seen from both experimental and theoretical results that the output voltage increases as the impact velocity increases. This can be explained through the analytical model that a larger λ results in a larger δ (see Fig. 5(b)) and then a larger A_b when other parameters are kept constant, hence, a larger output voltage can be achieved according to (11). Therefore, the feasibility of the theoretical approach in analyzing the influences of the impact velocity on the system output voltage is demonstrated. Next, the system output voltages under different impact velocities are presented in Fig. 8(b), where the input voltage was $U_i = 2000$ V and the pre-stretched ratio was $\lambda = 3$. Again, although the experimental output voltage is smaller than the theoretical one, the same increasing trend of the theoretical and experimental output voltages following the increase of impact velocity, which results from the positive correlations between the U_o, A_b, δ and v_A (See (11) and (21)), verifies the feasibility of the analytical model in analyzing the influence of the impact velocity on the system output voltage. Last, in Fig. 8(c) the system output voltages under different input voltages are presented, where $\lambda = 3$ and $H_A = 100$ mm ($v_A = 1.4$ m/s) were pre-set in the theoretical analysis and experiments. It is found that the experimental output voltage increases as the input voltage increases, and this trend accords with the theoretical results, which can be easily understood from (11). Thus, the feasibility of the analytical model in analyzing the influence of the input voltage on the system output voltage can be verified.

Moreover, the energy conversion efficiencies under different parameteric conditions are obtained theoretically and experimentally and are presented in Fig. 8(d-f). It can be seen from Fig. 8(d) that η increases as λ increases. This accords with our previous analysis that a larger λ reduces the energy dissipation during the deformation and revovery

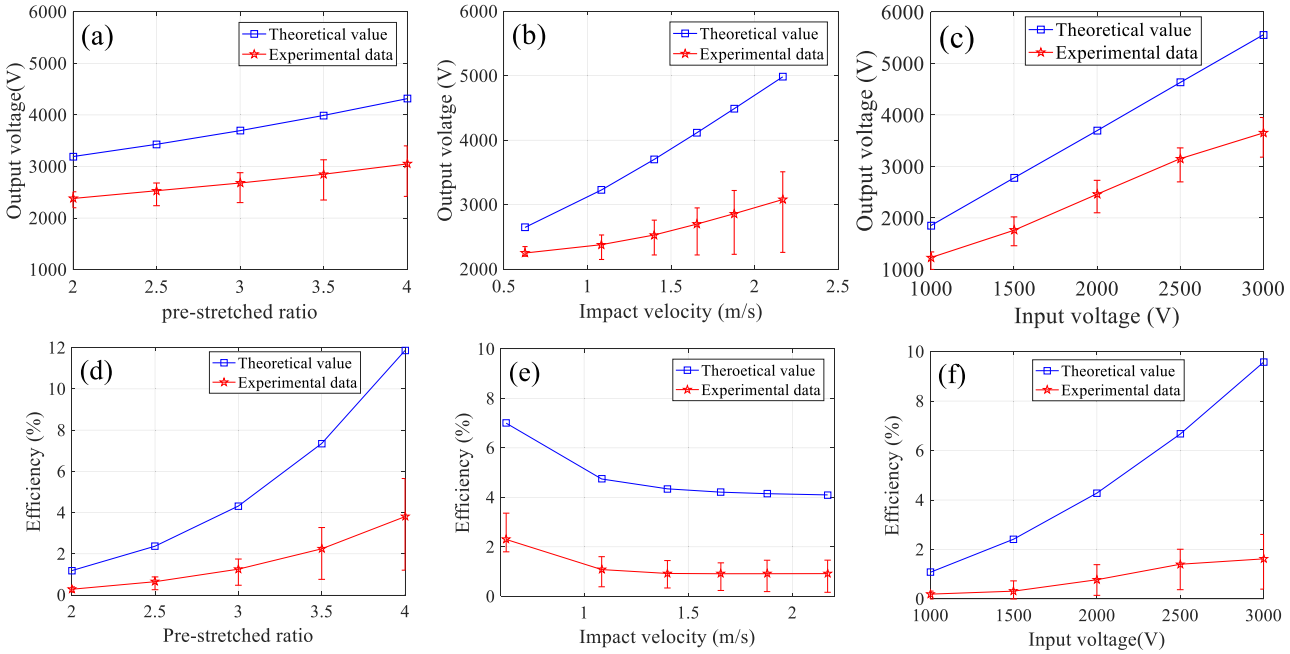

FIGURE 8. Output voltage against (a) pre-stretched ratio ($H_A = 100$ mm ($v_A = 1.4$ m/s), $U_i = 2000$ V), (b) impact velocity ($\lambda = 3$, $U_i = 2000$ V) and (c) input voltage ($\lambda = 3$, $H_A = 100$ mm ($v_A = 1.4$ m/s)).

process, thus enhancing the energy conversion efficiency. Fig. 8(e) tells that η presents a decreasing trend as v_A increases. This can be explained from our previous analysis that a larger inpact velocity results in more energy dissipation during the deformation and recovery process, thus decreasing the energy conversion efficiency. Last, one can see from Fig. 8(f) that η increases with the increasing of U_i. This can be easily understood from (16) that η and U_i have a positive correlation. However, it should be pointed out that as U_i increases, the difference between the theoretical and experimental output voltages results in a higher difference between the theoretical and experimental energy conversion efficiencies (See Fig. 8(c, f)), which can be explained from the square term of U_o in (16). Overall, it can be seen from Figs. 8(d-f) that, as the experimental output voltages are lower than the theoretical ones, the energy conversion efficiencies obtained from experiments are lower than those obtained from theoretical analysis. However, the same trends between the theoretical and experimental curves shown in Fig. 8(e-f) demonstrate that the analytical model is suitable to analyze the influences of different parameters on the system energy conversion efficiency.

IV. SIMULATIONS AND DISCUSSION

In Section II, the calculation approaches for the electrical outputs and energy conversion efficiency of the SSI model at its first impact are derived. The determination method for the parameters of r and δ under certain impact conditions are obtained in Section III, and the system output voltages and the energy conversion efficiencies are measured through experiments to verify the feasibility of analytical model. Thus, the influences of different parameters including the pre-stretched ratio, impact velocity, and input voltage on the impact-based energy conversion performance can be further obtained through simulations. The simulation results, which are obtained from the Matlab software, are presented and analyzed in this section.

What should be first stated is that the following parameters were given for the simulations in this section unless stated otherwise:

$$\lambda = 3, \quad Te = 25^{\circ}\text{C}, \ \varepsilon_r = 4.69, \ v_A = 1.4 \text{ m/s}, \\ U_i = 2000 \text{ V}, \quad m = 3.5 \text{ g} \tag{22}$$

In this paper, the DEM specimens were fabricated using a raw DEM with mass $M_0 = 0.75$ g, radius $R_0 = 15$ mm, and thickness $h_0 = 1$ mm. Therefore, the effective mass and volume of the specimen with radius $R = 6$ mm and thickness $h = h_0/\lambda^2$ can be calculated as:

$$\begin{cases} M = \dfrac{\pi R^2 h}{\pi R_0^2 h_0} M_0 = \dfrac{\pi R^2 (h_0/\lambda^2)}{\pi R_0^2 h_0} M_0 = \dfrac{36}{225\lambda^2} M_0 \\ V = \pi R^2 h = \dfrac{36\pi}{\lambda^2} \end{cases} \tag{23}$$

A. INFLUENCE OF THE PRE-STRETCHED RATIO ON THE ENERGY CONVERSION PERFORMANCE

We have learnt that the values of ε_r, r and δ are affected by λ when other parameters are kept constant. Thus, the pre-stretched ratio λ must influence the impact-based energy conversion performance, which is studied in this subsection by calculating the electrical outputs and energy conversion efficiency.

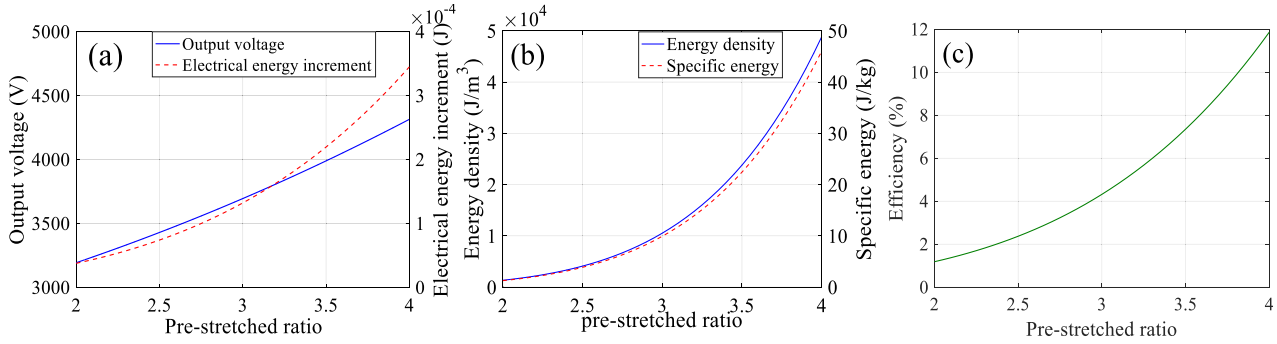

FIGURE 9. (a) Output voltage and electrical energy increment of the DEG against the pre-stretched ratio; (b) energy density and specific energy of the DEG against the pre-stretched ratio; (c) energy conversion efficiency against the pre-stretched ratio.

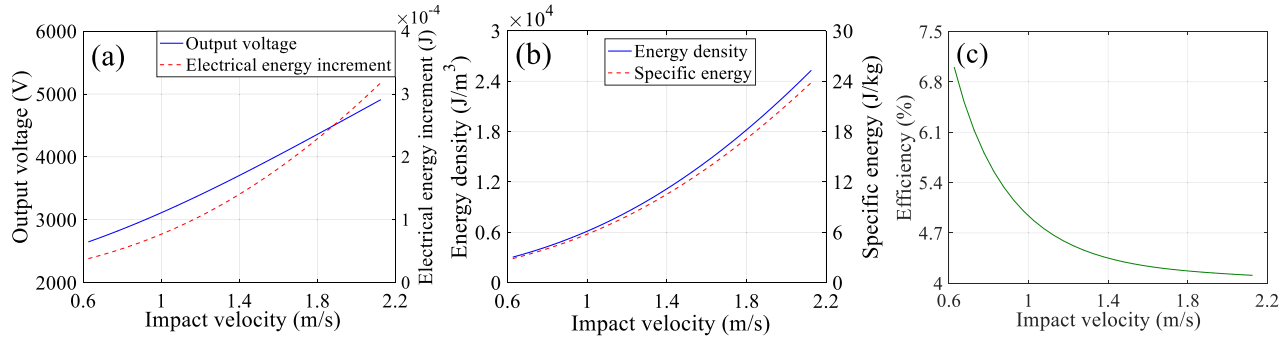

FIGURE 10. (a) Output voltage and electrical energy increment of the DEG against the impact velocity; (b) energy density and specific energy of the DEG against the impact velocity; (c) energy conversion efficiency against the impact velocity.

The simulation results are shown in Fig. 9. It can be seen from Fig. 9(a, b) that, as λ increases, U_o, ΔW, ED and SE all increase when other parameters such as v_A and U_i are kept constant. It is easy to imagine that as λ increases, the DEM is easier to be deformed under impacts, thus producing a larger δ according to (20) and a larger area A_b at the largest deformation of the DEM. On the other hand, the initial area A_c of the DEM is kept constant regardless of the value of λ. Thus, the output voltage U_o increases according to (11) and larger ΔW, ED and SE can be observed accordingly. These results indicate that increasing λ has a positive effect on the electrical outputs of the model.

Fig. 9(c) demonstrates an increasing trend of η with increasing λ, which is beneficial for energy harvesting. Although the energy conversion efficiency is not high under the conditions with the given parameters, it provides a feasible way to enhance the energy conversion efficiency of the impact-based DEG by increasing the pre-stretched ratio of the DEM to some extent.

B. INFLUENCE OF THE IMPACT VELOCITY ON THE ENERGY CONVERSION PERFORMANCE

We have learnt from (18) and (21) that the impact velocity v_A affects the COR and the largest deflection of the DEM, thus affecting the impact-based electrical outputs and energy conversion efficiency. The detailed influences are presented in Fig. 10 through several simulations. It can be seen from Fig. 10(a, b) that as v_A increases, all electrical outputs increase. These results can be explained from (21) that the higher the impact velocity v_A the higher the deflection δ and the thinner the thickness h_b, thus producing a higher output voltage U_o according to (11). Higher ΔW, ED and SE have been obtained accordingly.

On the other hand, the energy conversion efficiency η drops when v_A increases, as shown in Fig. 10(c). Although more electrical energy can be gained from a higher impact velocity, the energy conversion efficiency may decrease due to the increase of the kinetic energy loss. This should be taken into account in the further design of the impact-based DEGs especially on the occasions for high expected efficiency.

C. INFLUENCE OF THE INPUT VOLTAGE ON THE ENERGY CONVERSION PERFORMANCE

Last, the influence of the input voltage U_i on the impact-based energy conversion performance is studied through numerical simulations. The simulation results are shown in Fig. 11. It can be seen that all electrical outputs increase as the input voltage U_i increases. It can be seen from Fig. 5(e, f) that U_i has nothing to do with δ and also h_b. Thus, U_i is the only factor to affect the output voltage U_o according to the first equation of (11). Thus, the higher U_o the higher ΔW, ED and SE can be obtained under the increasing input voltage U_i.

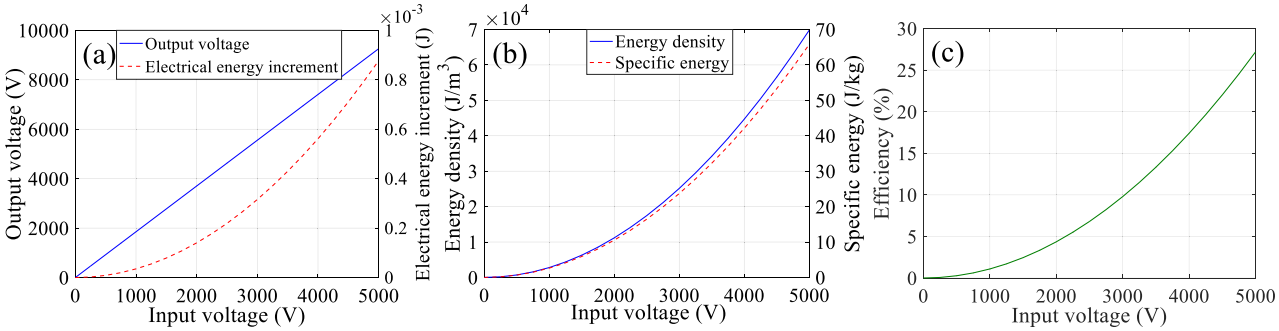

FIGURE 11. (a) Output voltage and electrical energy increment of the DEG against the input voltage; (b) energy density and specific energy of the DEG against the input voltage; (c) energy conversion efficiency against the input voltage.

Moreover, Fig. 11(c) tells that U_i has a positive effect to enhance the energy conversion efficiency of the DEG. It can be learnt from (19) that higher U_i results in lower r. Thus, a higher η can be obtained through (16). This provides a possible solution to enhance the energy conversion efficiency of the impact-based DEGs.

V. CONCLUSION

In this paper, a single-sided impact (SSI) model based on the free fall of a rigid ball was proposed to study the energy conversion mechanism and performance of a type of impact-based dielectric elastomer generators (DEGs). The impact-based energy conversion mechanism was revealed first by analyzing the energy conversion process according to energy conservation law, and the electrical outputs (including the output voltage, electrical energy increment, harvested energy density, and harvested specific energy) and the energy conversion efficiency were further derived. These parameters can provide reasonable indexes to evaluate the energy conversion performance of the proposed model. To calculate these indexes quantitatively, several key parameters, including the coefficient of restitution (COR) and the largest deflection at impacts, were determined through the impact experiments. It was found that the values of the COR and the largest deflection were decided by the pre-stretched ratio, impact velocity, and input voltage, and the empirical expressions to calculate their values were obtained. Thus, the electrical outputs and the energy conversion efficiency of the system were further obtained. Moreover, the output voltage measurement experiments were conducted to verify the theoretical approach in analyzing the system's electrical responses and the parameters' influences. Furthermore, the influences of the pre-stretched ratio, impact velocity, and input voltage on the energy conversion performance of the proposed SSI model were presented through simulations. It can be learnt that the appropriate adjustments of the above-mentioned parameters can enhance the system energy harvesting performance, thus benefiting the design and optimization of the impact-based DEGs under specific vibrational environments in the future work.

ACKNOWLEDGMENT

(Xi-Xin Rao and Li-Kuan Zhu contributed equally to this work.)

REFERENCES

[1] D. Huang, S. Zhou, and G. Litak, "Theoretical analysis of multi-stable energy harvesters with high-order stiffness terms," *Commun. Nonlinear Sci. Numer. Simul.*, vol. 69, pp. 270–286, Apr. 2019.

[2] S. P. Beeby, M. J. Tudor, and N. M. White, "Energy harvesting vibration sources for microsystems applications," *Meas. Sci. Technol.*, vol. 17, no. 12, pp. 175–195, 2006.

[3] F. K. Shaikh and S. Zeadally, "Energy harvesting in wireless sensor networks: A comprehensive review," *Renew. Sustain. Energy Rev.*, vol. 55, pp. 1041–1054, Mar. 2016.

[4] C. Dagdeviren, P. Joe, O. L. Tuzman, K.-I. Park, K. J. Lee, Y. Shi, Y. Huang, and J. A. Rogers, "Recent progress in flexible and stretchable piezoelectric devices for mechanical energy harvesting, sensing and actuation," *Extreme Mech. Lett.*, vol. 9, pp. 269–281, Dec. 2016.

[5] T. Y. Kim, J. Kwak, and B.-W. Kim, "Energy harvesting performance of hexagonal shaped thermoelectric generator for passenger vehicle applications: An experimental approach," *Energy Convers. Manage.*, vol. 160, pp. 14–21, Mar. 2018.

[6] J. Song and J. Wang, "Ferroelectric materials for vibrational energy harvesting," *Sci. China Technol. Sci.*, vol. 59, no. 7, pp. 1012–1022, Jul. 2016.

[7] C. R. Bowen, H. A. Kim, P. M. Weaver, and S. Dunn, "Piezoelectric and ferroelectric materials and structures for energy harvesting applications," *Energy Environ. Sci.*, vol. 7, no. 1, pp. 25–44, 2014.

[8] K. Fan, Y. Zhang, H. Liu, M. Cai, and Q. Tan, "A nonlinear two-degree-of-freedom electromagnetic energy harvester for ultra-low frequency vibrations and human body motions," *Renew. Energy*, vol. 138, pp. 292–302, Aug. 2019.

[9] J. Yang, Y. Wen, P. Li, and X. Bai, "A magnetoelectric-based broadband vibration energy harvester for powering wireless sensors," *Sci. China Technol. Sci.*, vol. 54, no. 6, pp. 1419–1427, Jun. 2011.

[10] Y. Zhang, T. Wang, A. Zhang, Z. Peng, D. Luo, R. Chen, and F. Wang, "Electrostatic energy harvesting device with dual resonant structure for wideband random vibration sources at low frequency," *Rev. Sci. Instrum.*, vol. 87, no. 12, Dec. 2016, Art. no. 125001.

[11] F. Wang and O. Hansen, "Electrostatic energy harvesting device with out-of-the-plane gap closing scheme," *Sens. Actuators A, Phys.*, vol. 211, pp. 131–137, May 2014.

[12] Z. L. Wang, "Triboelectric nanogenerators as new energy technology for self-powered systems and as active mechanical and chemical sensors," *ACS Nano*, vol. 7, no. 11, pp. 9533–9557, Nov. 2013.

[13] S. S. K. Mallineni, Y. Dong, H. Behlow, A. M. Rao, and R. Podila, "A wireless triboelectric nanogenerator," *Adv. Energy Mater.*, vol. 8, no. 10, 2018, Art. no. 1702736.

[14] S. Zhou and L. Zuo, "Nonlinear dynamic analysis of asymmetric tristable energy harvesters for enhanced energy harvesting," *Commun. Nonlinear Sci. Numer. Simul.*, vol. 61, pp. 271–284, Aug. 2018.

[15] W. Liu, Z. Yuan, S. Zhang, and Q. Zhu, "Enhanced broadband generator of dual buckled beams with simultaneous translational and torsional coupling," *Appl. Energy*, vol. 251, Oct. 2019, Art. no. 113412.

[16] H. Liu, J. Zhong, C. Lee, S.-W. Lee, and L. Lin, "A comprehensive review on piezoelectric energy harvesting technology: Materials, mechanisms, and applications," *Appl. Phys. Rev.*, vol. 5, no. 4, Dec. 2018, Art. no. 041306.

[17] M. N. Fakhzan and A. G. A. Muthalif, "Harvesting vibration energy using piezoelectric material: Modeling, simulation and experimental verifications," *Mechatronics*, vol. 23, no. 1, pp. 61–66, Feb. 2013.

[18] K. Yang, J. Wang, and D. Yurchenko, "A double-beam piezo-magneto-elastic wind energy harvester for improving the galloping-based energy harvesting," *Appl. Phys. Lett.*, vol. 115, no. 19, Nov. 2019, Art. no. 193901.

[19] L. Qi, H. Pan, S. Bano, M. Zhu, J. Liu, Z. Zhang, Y. Liu, and Y. Yuan, "A high-efficiency road energy harvester based on a chessboard sliding plate using semi-metal friction materials for self-powered applications in road traffic," *Energy Convers. Manage.*, vol. 165, pp. 748–760, Jun. 2018.

[20] G. Hu, J. Wang, Z. Su, G. Li, H. Peng, and K. C. S. Kwok, "Performance evaluation of twin piezoelectric wind energy harvesters under mutual interference," *Appl. Phys. Lett.*, vol. 115, no. 7, Aug. 2019, Art. no. 073901.

[21] J. Wang, G. Hu, Z. Su, G. Li, W. Zhao, L. Tang, and L. Zhao, "A cross-coupled dual-beam for multi-directional energy harvesting from vortex induced vibrations," *Smart Mater. Struct.*, vol. 28, no. 12, 2019, Art. no. 12LT02.

[22] J. Wang, S. Zhou, Z. Zhang, and D. Yurchenko, "High-performance piezoelectric wind energy harvester with Y-shaped attachments," *Energy Convers. Manage.*, vol. 181, pp. 645–652, Feb. 2019.

[23] D. Huang, S. Zhou, and Z. Yang, "Resonance mechanism of nonlinear vibrational multistable energy harvesters under narrow-band stochastic parametric excitations," *Complexity*, vol. 2019, Dec. 2019, Art. no. 1050143.

[24] D. Huang, S. Zhou, Q. Han, and G. Litak, "Response analysis of the nonlinear vibration energy harvester with an uncertain parameter," *Proc. Inst. Mech. Eng. K, J. Multi-Body Dyn.*, vol. 234, no. 2, pp. 393–407, 2019.

[25] B. Yan, N. Yu, L. Zhang, H. Ma, C. Wu, K. Wang, and S. Zhou, "Scavenging vibrational energy with a novel bistable electromagnetic energy harvester," *Smart Mater. Struct.*, vol. 29, no. 2, Feb. 2020, Art. no. 025022.

[26] P. Pan, D. Zhang, X. Nie, and H. Chen, "Development of piezoelectric energy-harvesting tuned mass damper," *Sci. China Technol. Sci.*, vol. 60, no. 3, pp. 467–478, Mar. 2017.

[27] T. G. McKay, B. M. O'Brien, E. P. Calius, and I. A. Anderson, "Soft generators using dielectric elastomers," *Appl. Phys. Lett.*, vol. 98, no. 14, Apr. 2011, Art. no. 142903.

[28] L. J. Romasanta, M. A. Lopez-Manchado, and R. Verdejo, "Increasing the performance of dielectric elastomer actuators: A review from the materials perspective," *Prog. Polym. Sci.*, vol. 51, pp. 188–211, Dec. 2015.

[29] N. Wang, C. Cui, H. Guo, B. Chen, and X. Zhang, "Advances in dielectric elastomer actuation technology," *Sci. China Technol. Sci.*, vol. 61, no. 10, pp. 1512–1527, Oct. 2018.

[30] S. Shian, K. Bertoldi, and D. R. Clarke, "Dielectric elastomer based 'grippers' for soft robotics," *Adv. Mater.*, vol. 27, no. 43, pp. 6814–6819, 2016.

[31] J. A. Rogers, T. Someya, and Y. Huang, "Materials and mechanics for stretchable electronics," *Science*, vol. 327, no. 5973, pp. 1603–1607, Mar. 2010.

[32] J. S. Zhang, Y. Q. Wang, H. L. Chen, and B. Li, "Energy harvesting performance of viscoelastic polyacrylic dielectric elastomers," *Int. J. Smart Nano Mater.*, vol. 6, no. 3, pp. 162–170, 2015.

[33] C. Jean-Mistral, T. Vu Cong, and A. Sylvestre, "Advances for dielectric elastomer generators: Replacement of high voltage supply by electret," *Appl. Phys. Lett.*, vol. 101, no. 16, Oct. 2012, Art. no. 162901.

[34] S. J. A. Koh, X. Zhao, and Z. Suo, "Maximal energy that can be converted by a dielectric elastomer generator," *Appl. Phys. Lett.*, vol. 94, no. 26, Jun. 2009, Art. no. 262902.

[35] T. G. McKay, S. Rosset, I. A. Anderson, and H. Shea, "Dielectric elastomer generators that stack up," *Smart Mater. Struct.*, vol. 24, no. 1, Jan. 2015, Art. no. 015014.

[36] M. El-hami, P. Glynne-Jones, N. M. White, M. Hill, S. Beeby, E. James, A. D. Brown, and J. N. Ross, "Design and fabrication of a new vibration-based electromechanical power generator," *Sens. Actuators A, Phys.*, vol. 92, nos. 1–3, pp. 335–342, Aug. 2001.

[37] G. Despesse, T. Jager, C. Jean Jacques, J. M. Léger, A. Vassilev, S. Basrour, and B. Charlot, "Fabrication and characterization of high damping electrostatic micro devices for vibration energy scavenging," in *Proc. Design, Test, Integr. Packag. MEMS MOEMS*, 2005, pp. 386–390.

[38] S. Roundy, P. K. Wright, and J. Rabaey, "A study of low level vibrations as a power source for wireless sensor nodes," *Comput. Commun.*, vol. 26, no. 11, pp. 1131–1144, Jul. 2003.

[39] E. Bortot and M. Gei, "Harvesting energy with load-driven dielectric elastomer annular membranes deforming out-of-plane," *Extreme Mech. Lett.*, vol. 5, pp. 62–73, Dec. 2015.

[40] D. Peter, R. Pichler, S. Bauer, and R. Schwödiauer, "Electrostatic converter with an electret-like elastomer membrane for large scale energy harvesting of low density energy sources," *Extreme Mech. Lett.*, vol. 4, pp. 38–44, Sep. 2015.

[41] G. Moretti, G. Malara, A. Scialò, L. Daniele, A. Romolo, R. Vertechy, M. Fontana, and F. Arena, "Modelling and field testing of a breakwater-integrated U-OWC wave energy converter with dielectric elastomer generator," *Renew. Energy*, vol. 146, pp. 628–642, Feb. 2020.

[42] Z. H. Lai, J. L. Wang, C. L. Zhang, G. Q. Zhang, and D. Yurchenko, "Harvest wind energy from a vibro-impact DEG embedded into a bluff body," *Energy Convers. Manage.*, vol. 199, Nov. 2019, Art. no. 111993.

[43] C. L. Zhang, Z. H. Lai, M. Q. Li, and D. Yurchenko, "Wind energy harvesting from a conventional turbine structure with an embedded vibro-impact dielectric elastomer generator," *J. Sound Vib.*, vol. 487, Nov. 2020, Art. no. 115616.

[44] C. Jean-Mistral and S. Basrour, "Scavenging energy from human motion with tubular dielectric polymer," *Electroactive Polym. Actuat. Devices*, vol. 7642, Apr. 2010, Art. no. 764209.

[45] C. L. Zhang, Z. H. Lai, X. X. Rao, J. W. Zhang, and D. Yurchenko, "Energy harvesting from a novel contact-type dielectric elastomer generator," *Energy Convers. Manage.*, vol. 205, Feb. 2020, Art. no. 112351.

[46] G. P. Rosati Papini, G. Moretti, R. Vertechy, and M. Fontana, "Control of an oscillating water column wave energy converter based on dielectric elastomer generator," *Nonlinear Dyn.*, vol. 92, no. 2, pp. 181–202, Apr. 2018.

[47] G. Moretti, G. P. R. Papini, M. Righi, D. Forehand, D. Ingram, R. Vertechy, and M. Fontana, "Resonant wave energy harvester based on dielectric elastomer generator," *Smart Mater. Struct.*, vol. 27, no. 3, Mar. 2018, Art. no. 035015.

[48] J. W. Zhang, Z. H. Lai, X. X. Rao, and C. L. Zhang, "Harvest rotational energy from a novel dielectric elastomer generator with crank-connecting rod mechanisms," *Smart Mater. Struct.*, vol. 29, no. 6, Jun. 2020, Art. no. 065005.

[49] Z. H. Lai, G. Thomson, D. Yurchenko, D. V. Val, and E. Rodgers, "On energy harvesting from a vibro-impact oscillator with dielectric membranes," *Mech. Syst. Signal Process.*, vol. 107, pp. 105–121, Jul. 2018.

[50] D. Yurchenko, Z. H. Lai, G. Thomson, D. V. Val, and R. V. Bobryk, "Parametric study of a novel vibro-impact energy harvesting system with dielectric elastomer," *Appl. Energy*, vol. 208, pp. 456–470, Dec. 2017.

[51] G. Thomson, D. Yurchenko, D. V. Val, and Z. Zhang, "Predicting energy output of a stochastic nonlinear dielectric elastomer generator," *Energy Convers. Manage.*, vol. 196, pp. 1445–1452, Sep. 2019.

[52] L. Serdukova, R. Kuske, and D. Yurchenko, "Stability and bifurcation analysis of the period-T motion of a vibroimpact energy harvester," *Nonlinear Dyn.*, vol. 98, no. 3, pp. 1807–1819, Nov. 2019.

[53] G. Thomson, Z. Lai, D. V. Val, and D. Yurchenko, "Advantages of nonlinear energy harvesting with dielectric elastomers," *J. Sound Vib.*, vol. 442, pp. 167–182, Mar. 2019.

[54] J. Zhou, L. Jiang, and R. E. Khayat, "Methods to improve harvested energy and conversion efficiency of viscoelastic dielectric elastomer generators," *J. Appl. Phys.*, vol. 121, no. 18, pp. 246–253, 2017.

[55] D. Yurchenko, D. V. Val, Z. H. Lai, G. Gu, and G. Thomson, "Energy harvesting from a DE-based dynamic vibro-impact system," *Smart Mater. Struct.*, vol. 26, no. 10, Oct. 2017, Art. no. 105001.

[56] J. Sheng, H. Chen, B. Li, and Y. Wang, "Influence of the temperature and deformation-dependent dielectric constant on the stability of dielectric elastomers," *J. Appl. Polym. Sci.*, vol. 128, no. 4, pp. 2402–2407, May 2013.

[57] J. Zhang, H. Chen, J. Sheng, L. Liu, Y. Wang, and S. Jia, "Constitutive relation of viscoelastic dielectric elastomer," *Theor. Appl. Mech. Lett.*, vol. 3, no. 5, 2013, Art. no. 054011.

[58] P. Mueller, R. Boettcher, A. Russell, M. Truee, and J. Tomas, "A novel approach to evaluate the elastic impact of spheres on thin plates," *Chem. Eng. Sci.*, vol. 138, pp. 689–697, Dec. 2015.

[59] Y. Jiang, S. Liu, M. Zhong, L. Zhang, N. Ning, and M. Tian, "Optimizing energy harvesting performance of cone dielectric elastomer generator based on VHB elastomer," *Nano Energy*, vol. 71, May 2020, Art. no. 104606.

XI-XIN RAO was born in Jiujiang, China, in 1965. He received the B.Eng. degree from the Jiangxi University of Technology, China, in July 2005, the master's degree from the Nanjing University of Aeronautics and Astronautics, China, in March 1992, and the Ph.D. degree in mechatronics engineering from Nanchang University, China, in November 2011.

He currently works as a Professor with the School of Mechanical Engineering, Nanchang University, China. He has published over 20 articles. His research interests include the design and machining of ME products, 3D printing, and vibration energy harvesting.

CAI-LIANG ZHANG was born in Ganzhou, China, in 1996. He received the B.Eng. degree in mechanical engineering from East China Jiaotong University, China, in July 2017, and the M.S. degree in mechanical engineering from Nanchang University, China, in June 2020.

His research interests include mechanical fault diagnosis and innovative small-scale high-efficiency vibration energy harvesters.

LI-KUAN ZHU was born in Tangshan, China, in 1985. He received the bachelor's degree from the Lanzhou University of Technology, China, in July 2009, and the master's and Ph.D. degrees in mechanical engineering from the Harbin Institute of Technology, China, in April 2018.

He currently works as an Assistant Professor with the College of Mechatronics and Control Engineering, Shenzhen University, China. He has published over ten articles. His research interests include micro electric machining technology, computational fluid mechanics, and intelligent manufacturing technology.

GUO-QING ZHANG was born in Zhalantun, China, in 1982. He received the B.Eng. degree from the Daqing Petroleum Institute, China, in July 2005, the master's degree from the Shenzhen Graduate School, Harbin Institute of Technology, China, in January 2009, and the Ph.D. degree in philosophy from The Hong Kong Polytechnic University, Hong Kong, in October 2014.

From October 2014 to June 2015, he worked as a Research Associate with The Hong Kong Polytechnic University. After 2015, he worked with the College of Mechatronics and Control Engineering, Shenzhen University, China. He is currently an Associate Professor with Shenzhen University, who has published over 50 articles and holds more than 20 granted patents in China and USA. His research interests include ultra-precision machining, mechanical fault diagnosis, and robotics.

JIAN-WEI ZHANG was born in Yichun, China, in 1995. He received the B.Eng. degree in mechanical engineering from East China Jiaotong University, China, in July 2017, and the M.S. degree in mechanical engineering from Nanchang University, China, in June 2020. He is currently pursuing the Ph.D. degree with Zhejiang University, China.

His research interests include mechanical fault diagnosis and vibration energy harvesting.

ZHI-HUI LAI was born in Ganzhou, China, in 1989. He received the B.Eng. degree and the master's and Ph.D. degrees in mechanical engineering from Tianjin University, Tianjin, China, in July 2010 and January 2015, respectively.

From January 2015 to June 2018, he worked as a Lecturer with the School of Mechatronics Engineering, Nanchang University, China. From September 2016 to September 2017, he was a Visiting Scholar with the Department of Mechanical Engineering, Heriot–Watt University, Edinburgh, U.K. He currently works as an Assistant Professor with the College of Mechatronics and Control Engineering, Shenzhen University, China. He has published over 30 articles. His research interests include weak-signal detection, mechanical fault diagnosis, and vibration energy harvesting.